ENGINEERING MECHANICS 2004
NATIONAL CONFERENCE
with international participation
Svratka, Czech Republic, 10 - 13 May 2004

VISUALIZATION AND NUMERICAL STUDY OF CONFINED COAXIAL JETS

Zdeněk Trávníček*, Jan Hrubý*, Jiří Vogel**

Summary: *This study deals with the limiting geometry of confined coaxial jets when the outer diameter of the annular jet is identical with that of the confining round duct. The study is a step in the development of a new method of investigation of aerosol formation out of gaseous precursors. The visualization was made in air, the numerical simulation used software FLUENT. The study focused on laminar flows, and on the stability loss of the inner round jet. A series of flow patterns is presented and the result is comparable with a classification known from available literature. Certain differences in scenarios of the patterns were observed such as three-dimensional structures and helical modes. To portrayal these structures, a stereoscopic technique was employed. The passing frequency was evaluated stroboscopically.*

1. Introduction

The confined coaxial fluid jets were investigated at the limiting geometry when the outer diameter of the annular jet is identical with that of the confining round duct. This geometry, the coordinate system and the present experimental arrangement are shown in Fig. 1. The arrangement is sometimes referred in literature as the merging flow in coaxial cylindrical pipes (Blyth & Mestel, 2001) or the laminar Craya-Curvet jets (Revuelta *et al*. 2004). Although problems of flow stability downstream the trailing edge of the inner pipe seem to be very interesting from both the fundamental and engineering application point of view, available literature exhibits a great lack of information. A rare example is the conference paper (Gore & Crowe, 1988) discussing the behavior of the laminar flow field near the stability loss. Eight distinct flow regimes were identified by visualization experiments. The present paper describes a new investigation based on experimental and numerical approaches.

Flow field regimes. The flow field is classified by three parameters (Gore & Crowe, 1988): d/D, U_i/U_o and Re_i; where d and D are the inner and outer diameters (see Fig. 1), respectively. Further, U_i and U_o are the average velocities in the inner (round) and outer (annular) jets, respectively, and the Reynolds number is defined from the inner pipe flow $Re_i = U_i\, d/\nu$. Fig. 2 shows a map of parameters related to the flow regimes I to VIII.

* Ing. Zdeněk Trávníček, CSc., Ing. Jan Hrubý, CSc., Institute of Thermomechanics, Academy of Sciences of the CR, Dolejškova 5, 182 00 Prague 8; Tel.: +420-26605 3302; fax: + 420-28658 4695; e-mail: tr@it.cas.cz, hruby@it.cas.cz.
** Doc. Ing. Jiří Vogel, CSc., Czech Technical University in Prague, Technická 4, 166 07 Prague 6; Tel.: +420-22435 2669; fax: + 420-22431 0292; e-mail: vogel@fsid.cvut.cz.

The qualitative classification according to (Gore & Crowe, 1988) is following:

I Flow becomes turbulent shortly after leaving the inner jet.

II An appreciable laminar section before the onset of turbulent flow.

III A short laminar section before transition occurs, the flow initially *curves inward*.

IV Initially laminar flow rapidly becomes turbulent dispersing the tracer quickly; the faster outer fluid forms characteristic *long fingers* of the inner (slower) fluid pointing outward and in the downstream direction.

V Pseudo-turbulent flow; large eddies are formed *without rapid* (turbulent) *mixing*.

VI Long laminar section preceding transition to turbulent flow – similarly as II, but the tracer expands more rapidly.

VII Very similar to regions VI, except *a very slight back-flow* (visualized by the tracer) *along the duct wall.* After short time (~minutes) the entire volume near the wall is filled with tracer.

VIII Complete laminar flow and very little mixing.

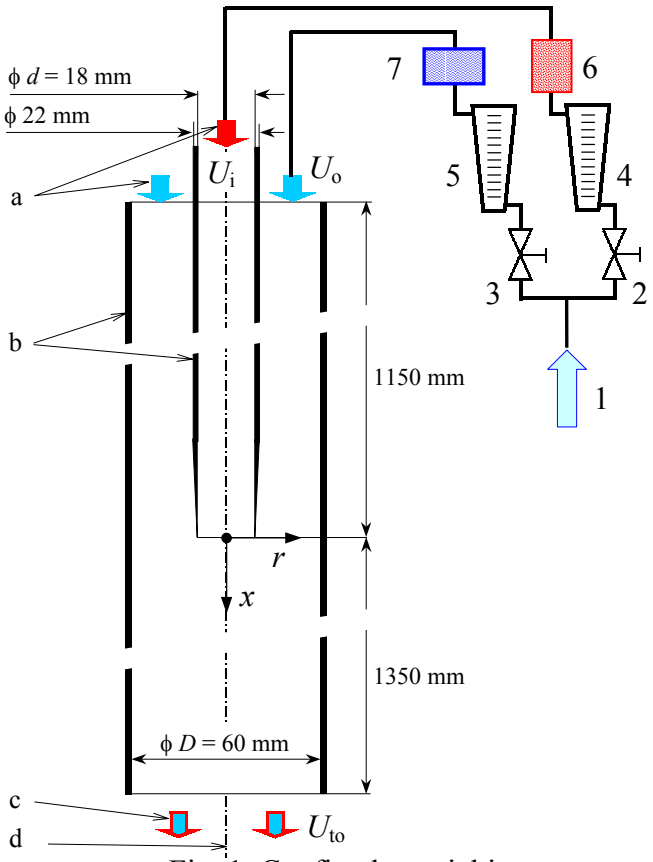

Fig. 1. Confined coaxial jet

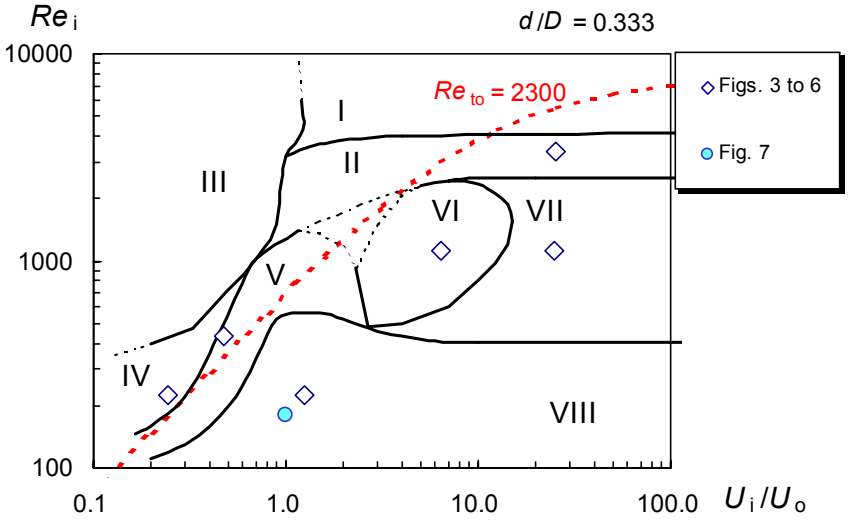

Fig. 2. Map of parameters related to the flow regimes I to VIII (Gore & Crowe, 1988); points denote experiments, which are discussed in this paper.

The dotted curve $Re_{to} = 2300$ in Fig. 2 shows the critical Reynolds number of turbulence transition in the developed pipe flow, after mixing of the both inner and outer flows (a well known value 2300 is considered here). This curve can be derived from the continuity equation and from the definitions of the both Reynolds numbers $Re_i = U_i\, d/\nu$ and $Re_{to} = U_{to}\, d/\nu$, where U_{to} is the (total) average velocity in the outlet (see Fig. 1):

$$\mathrm{Re_i} = \mathrm{Re_{to}} \frac{1}{\left(\frac{d}{D}\right)\left(\frac{U_i}{U_o}\right) + \frac{D}{d} - \frac{d}{D}} \qquad (1)$$

Further, points in Fig. 2 show parameters of the present experiments, they will be discussed below.

Motivation. At some atmospheric conditions, bursts of new aerosol particles (the so-called secondary aerosol) have been observed (*e.g.* Mäkela *et al.*, 1997). This phenomenon is important especially because of the influence of the atmospheric aerosols on the global climate evolution. The mechanism of the formation (nucleation) of the secondary aerosol particles is unknown. Traditional hypothesis is that the nucleation is due to interaction of (mainly) water and sulfuric acid vapors. Sulfuric acid forms in the atmosphere by consecutive photo-oxidation of sulfur, which enters the atmosphere in volcanic eruptions or as a product of burning of fossil fuels. Understanding the process of water-sulfuric acid nucleation appears a great challenge to both experimentalists (Wyslouzil *et al.*, 1991) and theorists (Noppel *et al.,* 2002). We develop a new experimental method, based on laminar mixing (by molecular diffusion) of two vapor-saturated airflows. The inner flow is saturated with sulfuric acid vapor, and the outer flow is saturated with water vapor. Because of the strongly non-ideal thermodynamic behavior of the two components, the system becomes supersaturated after mixing, and new particles are formed by binary homogeneous nucleation. In the laminar flow field, the concentration profiles can be computed with good accuracy. By measuring the integral rates of particle production and by reconstructing the concentration (humidity and acidity) fields using numerical simulation (studied in this work), the dependence of the nucleation rate on the humidity, acidity, and temperature can be determined. Such knowledge is needed for assessing the relevance of the water-sulfuric acid nucleation for environmental application. In order that the laminar flow model corresponds to reality, the flow must be stable. The existence of the trailing edge at the end of the inner tube makes the question of flow stability highly nontrivial. Therefore, a large part of this work is devoted to this problem.

2. Experimental methods

Fig. 1 shows a schematic view on the present experimental setup. The entire facility is situated vertically and connected to pressurized air supply (1) through two flow branches. The inner and outer airflow rates are controlled by the throttle valves (2, 3) and measured by rotameters (4, 5) respectively. The average velocities U_i and U_o are calculated from the airflow rates.

The present flow visualization was made by a home-made fog/smoke generator 6. Optionally, either water fog or cigarette smoke were employed. Further, the outer jet supply

was equipped width a home-made humidifier 7 to investigate an influence of air humidity gradient on the shear layer stability. Typical air temperature and humidity were, respectively, 25°C and 35% without the humidification, or 23°C and (75-85)% with the humidification.

An illumination was made by a flashlight. Contrasting white streaklines on black background were observed and photographed by a digital camera (OLYMPUS 2500). To investigate three-dimensional effects, a stereoscopic technique was employed: a pair of identical digital cameras were located at azimuthal angle 90° one towards other. Since both camera shutters were open for a relatively long time (0.25s), the single flashlight guaranteed a synchronization of both photographs.

3. Numerical simulation

The fluid flow is assumed to be incompressible, isothermal, laminar, and stationary. The fluid properties (density and viscosity) are assumed to be constant. With these simplifications, two equations govern the mean velocity flow field: continuity and momentum (Navier–Stokes) equations. Moreover, to model mass transfer of multicomponent and multiphase flow including a condensation, mass transport equations of contaminant *h* (water vapor in the annular jet) and *a* (acid coming through the inner jet) were solved too.

The flow field is computed with the commercial finite-volume code FLUENT, in implicit formulation, in absolute velocities. Continuity and momentum equation are coupled by the SIMPLE algorithm, which works in predictor–corrector steps, (Patankar, 1980). As a solver were used the segregated solver which has been traditionally used for incompressible and mildly compressible flows. A standard scheme is used for the pressure discretisation, and first order upwind is used in the momentum. The multi-grid method to accelerate the convergence, and iterative technique with under-relax predictions of the velocity and pressure are used. Default under–relaxation factors of the solver were used, which were 0.3 and 0.7 for the pressure and momentum, respectively. The results of iterations were evaluated by means of convergence criteria based on residual evolutions. The solution was considered to be converged when the sum of normalized residuals was less then $1 \cdot 10^{-3}$ with the exception of the water vapor and the acid where residuals have been less then $1\ 10^{-5}$. The present computations were performed using the common PC multiprocessor Silicon Graphic computer, and usually took from a half an hour to one hour for a task.

The domain, grid, boundary conditions, and input data. The geometry of the computational domain was used basically the same as at experiments (see Fig. 1). The unstructured axi-symmetrical grid of mixed cells had 3717 volumes and 39702 nodes. The prescribed boundary conditions (a–d) are plotted in the Fig. 1, and are as follows:

a) Inlets. Since the tube length was set to be long enough (64*d*), the velocity profiles at the inlets were set as uniform (velocities U_i, U_o). Three tasks with different ratio of inner/outer jet velocities were simulated: (A) $U_i/U_o = 0.5$, (B) $U_i/U_o = 1.0$, and (C) $U_i/U_o = 2.0$. The values U_i, U_o were given to satisfy approximately a condition $U_{to} = 0.03$ m/s, it means Re_{to}– value was approximately 120.
b) Walls: A no-slip boundary condition, i.e., all velocity components are zero.
c) Outlet: A static pressure was prescribed as reference value, 101325 Pa.
d) Nozzle axis: standard symmetry conditions were employed.

Fluid properties of working fluid (nitrogen): fluid density, fluid density as incompressible ideal gas; dynamic viscosity, $\mu = 1.72 \times 10^{-5}$ kg/(ms).

4.1 Visualization experiments – results and discussions

Fig. 3 shows typical flow patterns II, IV to VI (regimes I and III were out of possibilities of the present facility). These flow patterns are comparable with a classification given by (Gore & Crowe, 1988). The following paragraphs focus on four phenom which are not been referred in the available literature yet (in relation to the confined coaxial jets).

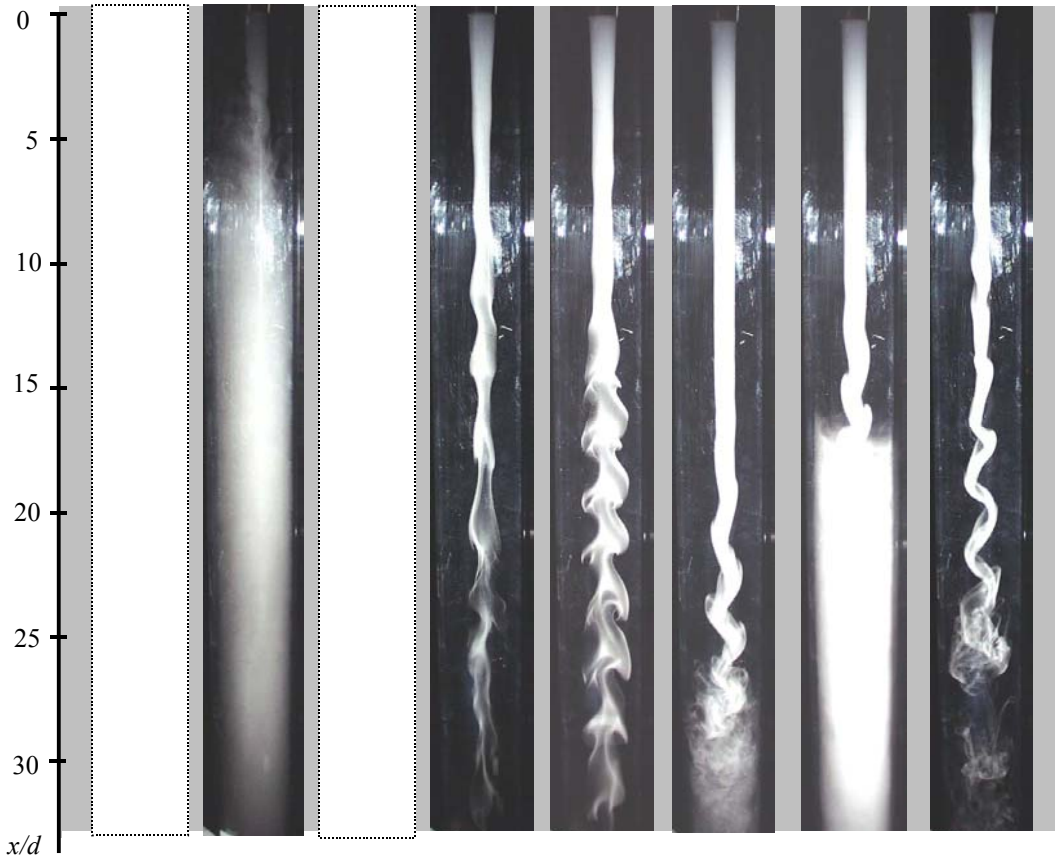

Regime	I	II	III	IV	V	VI	VII	VIII
U_i/U_o	---	25.5	---	0.24	0.48	6.43	24.6	1.25
Re_i	---	3380	---	224	436	1130	1130	224

Fig. 3. Visualisation of flow field in the denoted regimes.

Three-dimensional effects versus two-dimensional "polarization" of fluid columns. Figs. 4 and 5 demonstrate the effect of the two-dimensional "polarization" of the inner fluid jet during its stability losses. These pair of synchronized photographs were made by a pair of identical cameras (L, R), under identical parameters. Figs. 5 L, R were made a few minutes after Figs. 4 L, R. The instability of the jet columns is developed mainly in a specific plane (e.g., Fig. 4 R), however, a slow (or irregular) circumvolution of this plane occurs. After few minutes, the pattern is turn approximately by azimuthal angle 90^o as is demonstrated by comparison of Figs. 4 and 5.

Helical mode of the patterns. Figs. 6 L, R demonstrate a helical mode of the flow pattern, or the typical "corkscrew" face of this mode. It was frequently observed in the regime V, and it was very rare at the other regimes.

Vortex passing frequency. It is well know fact that the Strouhal number of the fundamental frequencies of unconfined axisymmetric jets vary from 0.3 to 0.6, and that the value of 0.3 is in tune with the most preferred mode (i.e. the most amplified mode obtained by an artificial external excitation) – see e.g. Crow & Champagne (1971). The passing frequency of the present task was evaluated stroboscopically, and the resultant values of Strouhal number ($St = f\,d/U_i$) ranged from 0.4 to 1.2 for $Re_i < 700$, in agreement with the expectation.

Effect of air humidity gradient on the shear layer stability. Four sets of experiments were made, which varied in the inner/outer jet fluid: (a) dry air with cigarette smoke/dry air, (b) water fog in practically saturated air/dry air, (c) dry air with cigarette smoke/humidified air, (d) water fog in practically saturated air/humidified air. Repeatedly, a stability of these combinations follow the mentioned order 1 – 4, e.g., the dry air jet was more stable then of the humidified one, and the coaxial jets humidification evidently decreases the stability of the pattern. This effect was demonstrated at Re_i = 144 and 180 with the same results, Figs. 7 shows typical results for Re_i = 180, at U_i/U_o = 1.01, i.e. in regime VIII.

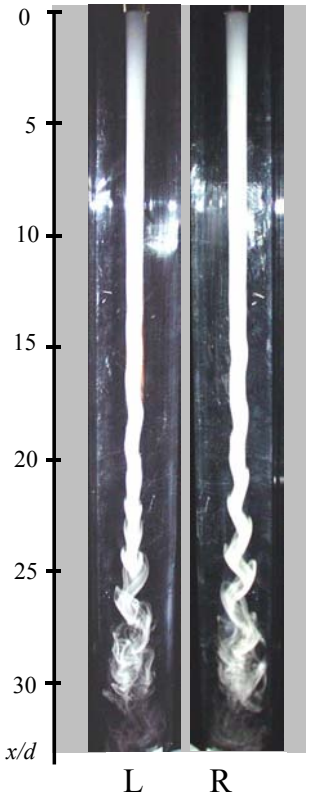

Fig. 4. Stereoscopic visualisation.

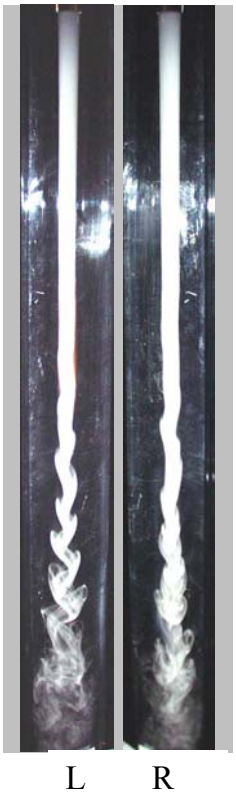

Fig. 5. Stereoscopic visualisation.

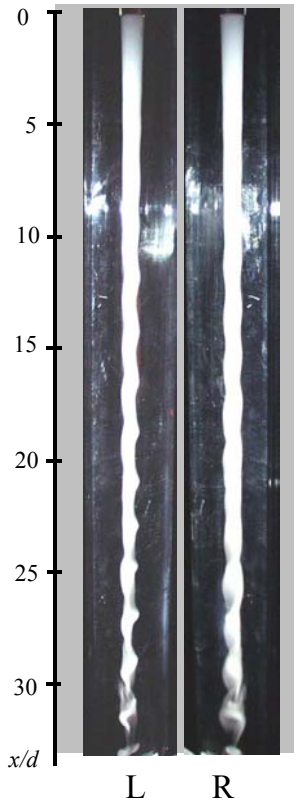

Fig. 6. Helical (or "corkscrew") mode of the regime V (Re_i = 436, U_i/U_o = 0.64)

The reason of the effect of destabilization by humidity can be linked either with density or enthalpy changes. Although density decrease caused by air humidification seems to be rather small (about 0.5% in the present experiments), it can cause these effects as a result of great receptivity of flow fields near stability losses. On the other hand, enthalpy increase may be even more significant, because the humidification technique causes quite big increase of enthalpy from 42 kJ/(kg of dry air) to 65–75 kJ/(kg of dry air), i.e. by 55% – 78% at the present experiments! It is fair to say here that an understanding of this effect is very far from complete, thus it remains an interesting challenge for the future.

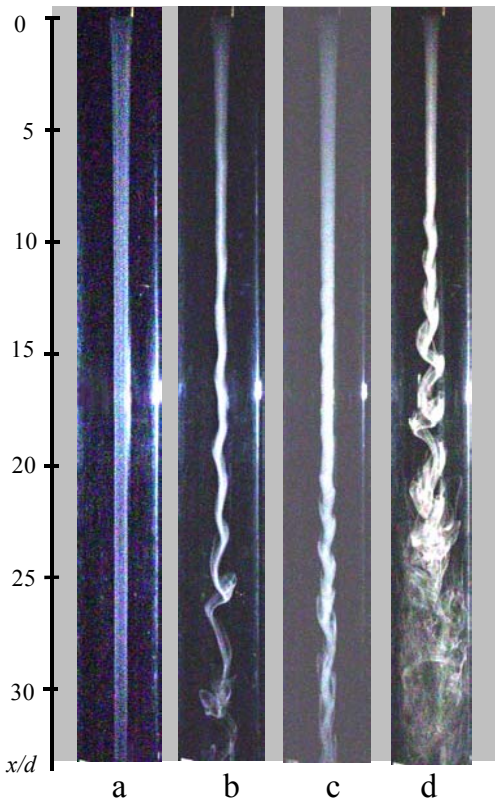

Fig. 7. Destabilization effect of air humidity.

4.2 Numerical simulation – results and discussions

Fig. 8 shows typical results as the flow field pathline for three simulated tasks A, B, and C. Fig. 9 shows concentration of the acid (coming from the inner jet) in a form of a distribution of the acidity in the mixture $Ra = p_a/p_{sa}$, where p_a is the actual partial pressure of acid, and p_{sa} (T) is the saturated vapor pressure of acid at given temperature. Similarly, Fig. 10 shows concentration of the water (coming from the annular jet) as the humidity of gas $Rh = p_h/p_{sh}$, where p_h is the actual partial pressure of water vapor, and p_{sh} (T) is the saturated pressure of water vapor at given temperature (only task B is shown here). The distribution of concentration of the both fractions, h and a, results in the nucleation rate (e.g., Wyslouzil *et al*., 1991), which is plotted in Fig. 11 for task B.

Fig. 12 shows computed velocity profiles for the tasks A, B, and C. Laminar mixing takes place predominantly at $x < 14d$, and the last two profiles $x = 14d$ and $44\ d$ are nearly the same (independently on the inlet boundary conditions, i.e., for the all three tasks. To illustrate this effect, Fig. 13 shows these velocity profiles in the spatial coordinates $r/d – x/d$.

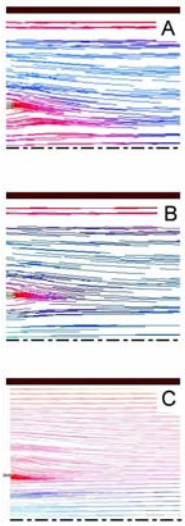

Fig. 8. Computed pathlines

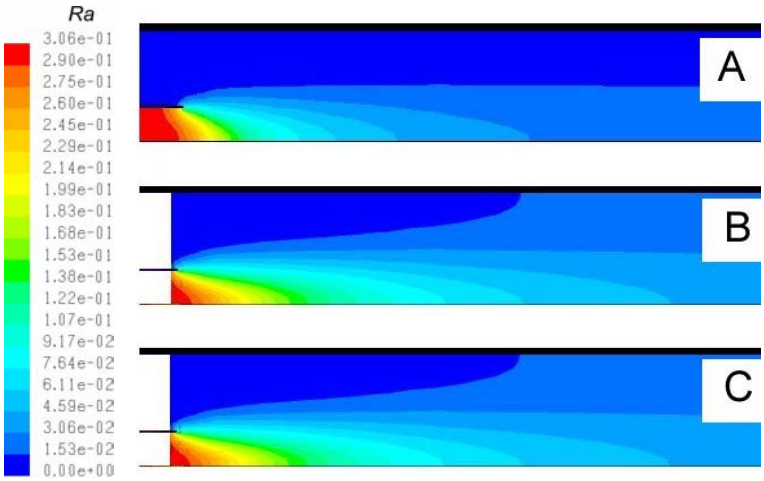

Fig. 9. Concentration of the acid.

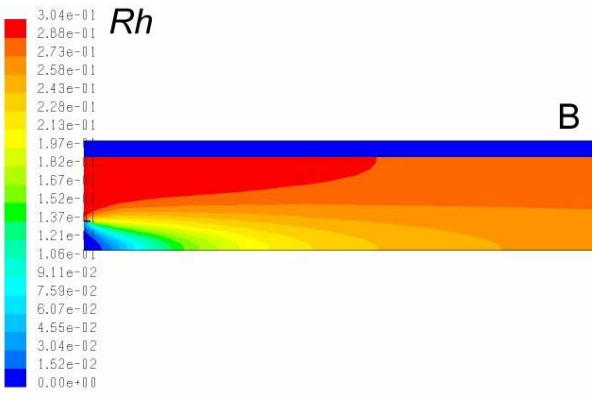

Fig. 10. Concentration of the water.

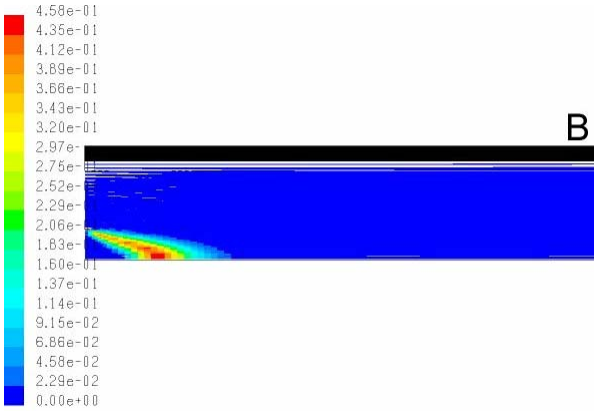

Fig. 11. nucleation rate

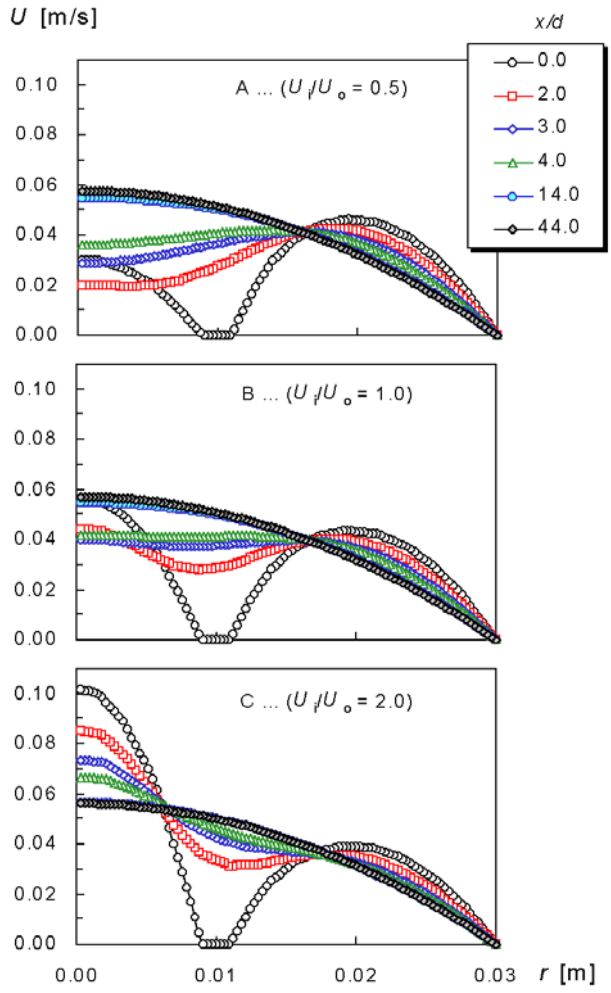

Fig. 12. Velocity profiles.

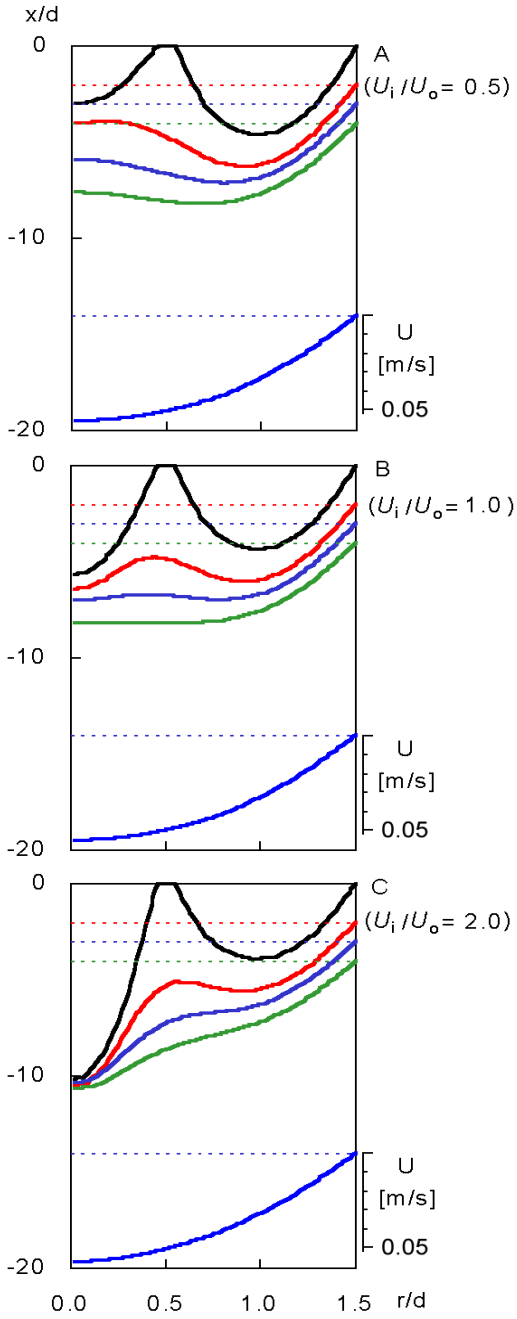

Fig. 13. Velocity profiles in the spatial coordinates.

5. Conclusions

Numerical and experimental investigations of laminar confined coaxial jets have been performed. The study focused on the limiting geometry when the outer diameter of the annular jet is identical with that of the confining round duct. The visualization was made in air, the numerical simulation used software FLUENT. This study is considered a step in the development of a new method of investigation of aerosol formation out of gaseous precursors.

Flow visualization demonstrated a series of flow patterns, and the result is comparable with a classification known from available literature. Certain differences in scenarios of the patterns were observed such as three-dimensional structures (two-dimensional "polarization" of fluid columns) and helical (or "corkscrew") modes. The passing frequency was evaluated stroboscopically, and Strouhal number was evaluated from 0.4 to 1.2; in agreement with the

expectation according to literature. Moreover, an effect of air humidity onto the stability was identified. The humidification causes a destabilization of the flow field. A possible explanation of this effect is supposed in relation with changes of fluid enthalpy, rather then simultaneous (and commonly referred) influence of fluid density.

Numerical simulation focused on laminar mixing of both jets for three typical tasks differing in the ratio of inner/outer jet velocities. The flow fields were computed, and examples of pathlines and velocity profiles are presented here. Further, spatial distributions of concentration (acidity and humidity) and the nucleation rates were computed.

The numerical simulation confirmed our prior conjecture (Hrubý, 2002) that nucleation occurs in a region resembling laminar flame. This situation is favorable for the purpose of the measurements. Visualization indicates that it is very difficult to find a regime, where the flow would be truly stable (without time-dependent component). In some conditions, the laminar region extends far from the end of the inner tube. It is sufficient when the flow remains (practically) stable within the "flame" area. The experiments indicate high susceptibility of the flow-field to minor disturbances. This fact will be respected in the design of the final experimental device for nucleation measurements.

6. Acknowledgments

We gratefully acknowledge the support by the Grant Agency of the Academy of Sciences of the Czech Republic (project No. A2076203).

7. References

Blyth, M.G. & Mestel, A.J. (2001) Merging flow in co-axial cylindrical pipes, *Q. Jl Mech. Appl. Math.,* 54, 4, pp.655-673.

Crow, S.C. & Champagne, F.H. (1971) Orderly structure in jet turbulence, *J. Fluid Mech.,* 48, pp.547-591.

Fluent User's Guide 6.1 (2002) Fluent 6.1 Documentation.

Gore, R.A. & Crowe, C.T. (1988) Observations on the flow in a confined coaxial jet, AIAA Paper No. 88-3591-CP 940-945.

Mäkelä, J. M., Aalto P., Jokonen, V., Pohja, T., Nissinen, A., Palmroth, S., Markkanen, T., Seitsonen, K., Lihavainen, H., Kulmala, M. (1997) Observations of ultrafine aerosol particle formation and growth in boreal forest. *Geophys. Res. Lett.* 24, pp. 1219-1222.

Noppel, M., Vehkamäki H., and Kulmala, M. (2002) An improved modell for hydrate formation in sulfuric acid-water nucleation. *J. Chem. Phys.* 116, pp.218-228.

Hrubý, J. (2002) Laminar co-flow tube for measurement of nucleation rates in atmospherically relevant systems. Unpublished.

Patankar, S.V. (1980) *Numerical Heat Transfer and Fluid Flow.* Hemisphere, Washington DC.

Revuelta, A., Martinez-Bazan, C., Sanchez, A. & Linan, A. (2004) Laminar Craya-Curvet jets, *Physics of Fluids,* 16, 1, pp.208-211.

Wyslouzil, B.E., Seinfeld, J.H., & Flagan R.C. (1991) Binary nucleation in acid-water system. II. Sulfuric acid-water and a comparison with mehanesulfonic acid-water, *J. Chem. Phys.*, 94, pp. 6842-6850.